Supporting information

Property		Value
Range of particle radii		0.1-1.0 mm
Particle density		2160×10^{9} kg/m^3
Model time step length		2.2×10^{-5} s
Start time of velocity loading		50,000 timesteps
Ramp up time of velocity loading		40,000 timesteps
Poisson's ratio of bonds		0.25
Internal friction of bonds		1.0
Normal stiffness of unbonded particles		10 GPa
Poisson's ratio of unbonded particles		0.25
Dynamic friction of unbonded particles		0.1
Static friction of unbonded particles		0.1
Normal stiffness of bonds	off-fault	10 GPa
	damage zone	5 GPa
	on-fault	1 GPa
Cohesion of bonds	off-fault	35 MPa
	damage zone	17 MPa
	on-fault	1 MPa

Table S1. Microparameters of particles and bonds found through calibration. We desire to simulate a bulk density ρ=2700 kg/m^3. Thus, we calculate the corresponding particle density using a representative model porosity, φ (20%), such that the particle density is ρ (1-φ), or 2160 kg/m^3. We then follow the established numerical technique of increasing the particle density by a factor of 10^9, which enables larger timestep lengths and thus shorter run times. Following the Courant condition, the minimum particle radius and maximum bond stiffness determine the timestep length. Each model has about 290,000 particles.

	Property
1	x-position
2	y-position
3	z-position
4	velocity component, v_x
5	velocity component, v_y
6	velocity component, v_z
7	divergence, first invariant of strain tensor, I_1
8	curl, $\nabla \times u$, where u the displacement field
9	second invariant of strain deviator tensor, J_2
10	normal strain, ε_{xx}
11	normal strain, ε_{yy}
12	normal strain, ε_{zz}
13	shear strain, ε_{xy}
14	shear strain, ε_{yz}
15	shear strain, ε_{zx}

Table S2. Features used in the models.

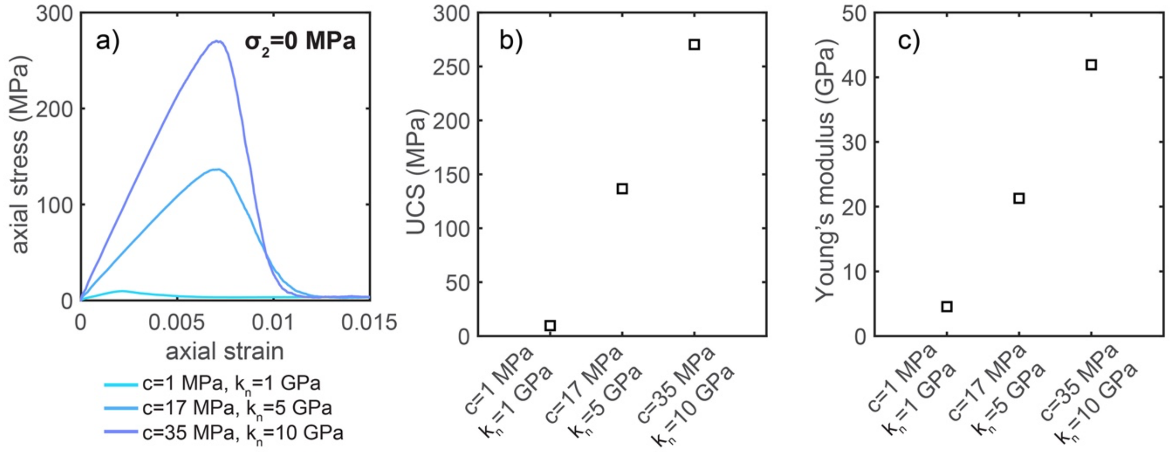

Figure S1. Calibration of the model microparameters in models in which all the bonds have the same set of microparameters. a) Macroscopic axial strain and axial stress during uniaxial compression tests on the homogeneous. b) Uniaxial compressive strength (UCS) of each model. c) Young's modulus of each model. We vary the cohesion, c, and bond normal stiffness, k_n, to achieve three distinct levels of damage, indicative of the fault zone, damage zone, and surrounding relatively intact host rock.

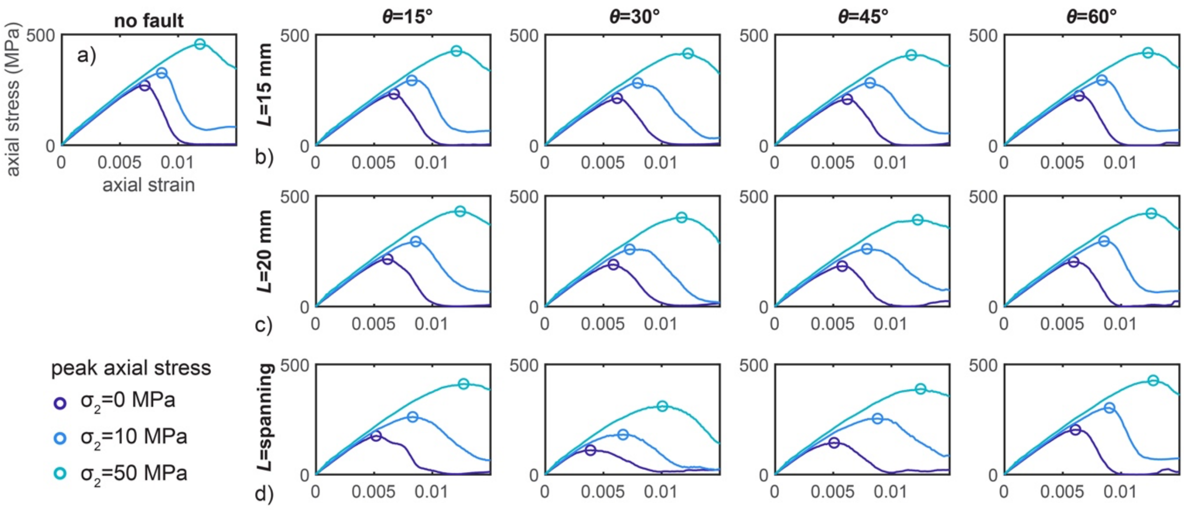

Figure S2. Macroscopic axial strain and axial stress acting on the simulation boundaries when the simulations do not include a fault (a), and include faults with L=15 mm (b), L=20 mm (c), and system-spanning faults (d). The columns in b-d) show the results when θ=15°, 30°, 45°, and 60°. The colors correspond to the applied confining stress, with σ_2=0 (dark blue), σ_2=10 MPa (blue), σ_2=50 MPa (light blue). The circles show the peak axial stress identified from the curves. The simulations include three phases of macroscopic stress accumulation due to the applied axial strain. First, the axial stress increases quasi-linearly with the axial strain, then the rate of axial stress accumulation slows, and finally the axial stress decreases.